

# Ultimate parameters of an all-optical $M_X$ resonance in Cs in ultraweak magnetic field

M.V. Petrenko<sup>✉</sup>, A.S. Pazgalev, and A.K. Vershovskii<sup>✉</sup>

*Ioffe Institute, St. Petersburg 194021, Russia*



(Received 13 July 2023; revised 25 August 2023; accepted 14 September 2023; published 29 September 2023)

We present the results of studying the parameters of the magnetic  $M_X$  resonance in an all-optical sensor built according to the two-beam Bell-Bloom scheme in nonzero ultraweak magnetic fields in which the effects of spin-exchange broadening suppression are partially manifested. We report on the features of the resonance under these conditions. We also optimize the resonance parameters to achieve maximum sensitivity in magnetoencephalographic sensors. We demonstrate an improvement in the ultimate achievable sensitivity of an all-optical  $M_X$  sensor by a factor of 4 or more, which in our experiment corresponds to a decrease from 13 to 3 fT/Hz<sup>1/2</sup> in a volume of 0.13 cm<sup>3</sup>. We also report the effect of incomplete suppression of spin-exchange broadening under conditions of strong transverse modulated optical pumping, and propose a semiempirical model to describe it.

DOI: 10.1103/PhysRevApplied.20.034074

## I. INTRODUCTION

This work is devoted to the search for promising ways to develop compact highly sensitive magnetic field (MF) sensors for the tasks of studying the magnetic activity of the brain (magnetoencephalography, MEG). This uniquely informative biomedical method, which appeared more than half a century ago, was not widely used for a long time, since the only types of sensors that provided the necessary sensitivity with sufficient compactness were superconducting quantum interference devices (SQUIDs) [1]. SQUID sensor arrays are extremely expensive, as is their annual maintenance; in addition, the SQUID sensors are separated from the object (human head) by a thick-walled dewar helmet, which significantly reduces the level of useful signal and limits the spatial resolution of the system.

The main competitor for SQUID appeared with the invention of optically pumped sensors using the spin-exchange relaxation-free (SERF) mode, which involves the suppression of spin-exchange broadening in a zero MF [2–6]. This caused an explosion of interest in MEG methods. SERF sensors are based on optical pumping and zero-field magnetic resonance (MR) line detection [3,5,7–10]. They do not require liquid helium cooling; they can be brought much closer to the head than SQUID sensors; they are capable of simultaneously measuring two or even three MF components. However, they also have disadvantages: an MEG array based on SERF is operable only if the field inhomogeneity in the volume does not exceed several tens of nanoteslas, and this nearly excludes the possibility of

working in relatively compact magnetic shields. In addition, each sensor modulates the MF in two or three [11] perpendicular directions, as a result of which the sensors operating in the array influence one another.

On the other hand, optically pumped nonzero field sensors (namely,  $M_X$  sensors) demonstrate parameters that are somewhat worse, but sufficiently suitable for use in MEG [12,13].  $M_X$  sensors do not use the SERF effect and measure not the MF components, but its modulus [10,14,15]. It should be noted here that in the presence of a nonzero constant field  $\mathbf{B}$ , such scalar sensors turn out to be sensitive only to the component of a weak signal that is parallel to  $\mathbf{B}$ ; consequently, in MEG, the  $M_X$  sensors turn out to be single-component with the sensitivity axis determined by the direction of the external field.  $M_X$  sensors, unlike SERF, can be “quiet,” meaning that they do not use either MF modulations or any other rf fields; they impose much lower requirements on the homogeneity of the MF; and due to the significantly larger width of the MR, they provide greater speed. In addition, the  $M_X$  signal is recorded at the Larmor frequency proportional to the MF, which makes it possible to transfer the signal frequency to a range free from low-frequency technical laser noise. Unfortunately, a wider MR linewidth to achieve the same level of sensitivity requires higher pump speeds—and therefore more powerful lasers, which, as a rule, cannot be integrated directly into the sensor (as is done in sensors using the SERF effect [7,16]).

In this paper, we explore the possibility of a compromise solution, namely, the use of an all-optical “quiet”  $M_X$  sensor built according to the Bell-Bloom scheme [12,14,17–19] in ultraweak MFs (meaning fields in which

\*Corresponding author. antver@mail.ioffe.ru

the SERF effect is already manifested, but the Larmor frequency still exceeds the linewidth). We demonstrate that such a sensor can show parameters similar to those of the SERF sensor without using MF modulation. At the same time, the MF required for such a sensor with an induction from one to several hundreds of nanotesla can be created both in a magnetically isolated room and in a magnetic shield, which promises a significant expansion of the field of application of the MEG. We demonstrate an improvement in the ultimate sensitivity (estimated from the MR parameters and shot noise) of the  $M_X$  sensor in ultraweak MFs by a factor of 4 or more, which in our particular scheme corresponds to an improvement from 13 to 3 fT/Hz<sup>1/2</sup> in a volume of 0.13 cm<sup>3</sup>.

This paper is organized as follows: in Sec. II, we describe the experimental setup and define the direction of the research. In Sec. III, we present the theoretical calculations that make it possible to estimate the dependence of the MR width on the MF and pump parameters. In Sec. IV, we present the data of the MR width measurement experiment and compare them with the data in Sec. III. In Sec. V, we examine the achievable ultimate sensitivity. In Sec. VI, we discuss our findings and present options for explaining the observed effects.

## II. EXPERIMENTAL SETUP

The study of the parameters of the MR was carried out in a magnetic shield [20] (Fig. 1). A cell with an internal size of  $8 \times 8 \times 8$  mm<sup>3</sup> filled with saturated Cs vapor and nitrogen at a pressure of 100 Torr was used as the sensitive element. The MF in the range of 60–2000 nT was created by a solenoid 90 cm long and 30 cm in diameter, the design of which included a pair of compensating coils. The field inhomogeneity in the cell volume did not exceed 0.5 nT. Cesium vapors were optically oriented by the pump

light emitted by an external cavity diode laser (VitaWave company). The MR signal was detected by the probe light emitted by a similar laser.

The experiment is carried out in the Voigt geometry: both beams, the pump beam and the detection (or probe) beam, were perpendicular to the MF and almost parallel to each other. Their Gaussian diameter was 4.9 mm, so that the pumped and detected volume was 0.13 cm<sup>3</sup> (which roughly corresponds to the volume of a cubic cell with a side of 5 mm). Part of the intensity of the detecting beam was split off on a translucent mirror TM and passed through the cell in the direction parallel to the magnetic shield axis (along vector **B**). This beam, shown in Fig. 1 by a dotted line, is used to align the MF vector in the shield [21] and is not part of the sensor circuit. The pump beam frequency is tuned to resonance with the  $D_1$  transitions of the cesium line, which connect the hyperfine level  $F = I - 1/2$  of the  $S_{1/2}$  state with the levels  $F' = I \pm 1/2$  of the  $P_{1/2}$  state [22,23]. The effective Zeeman pumping of the sublevel  $F = I + 1/2, m_F = F$  is partly due to the overlap of the optical absorption contours of two hyperfine transitions, and partly due to the conservation of the nuclear component of the momentum during collisions with buffer gas atoms in an excited state [22].

The MR was excited according to the Bell-Bloom scheme [12]: the polarization of the pump radiation was modulated by means of an EOM at a frequency close to the MR frequency: half a period, left-hand circular polarization; half a period, right-handed. A similar experimental geometry, but with an rf field, was used, for example, in Ref. [24].

At each temperature and/or at each MF value, we took an array of records at four values of the pump intensity and at four values of the detection intensity (16 records of the MR signal in total). The signals of rotation of the polarization azimuth of the probe beams were detected by balanced photodetectors PHD1 and PHD2, after which they were fed to Stanford Research SR830 synchronous detectors. The polarization azimuth rotation signal from the photodetector PHD2 was used as an error signal for zeroing the transverse-field components, which was carried out using a two-coordinate Helmholtz coils system [21,25,26]. For further processing, we used the polarization rotation signal from the PHD1 photodetector, which is proportional to the precessing transverse magnetization of the medium. Two quadrature ( $S_x$  and  $S_y$ ) components of the signal from the output of the synchronous detector were combined into a complex signal  $S_x + iS_y$  and approximated by a common Lorentzian contour with an arbitrary phase, while the complex bias was subtracted from them. Next, the obtained series were processed and the MR parameters were extrapolated to zero detection intensity. We also measured the total photocurrent at the output of a balanced photodetector PHD1, and, based on its value, calculated the spectral density of shot noise. Preliminary studies were carried out

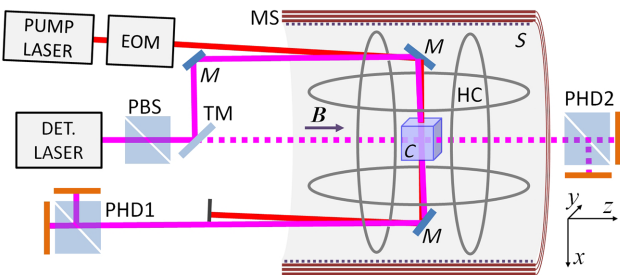


FIG. 1. A simplified experimental setup: PUMP LASER, a pump light source; DET. LASER, detection light source; EOM, electro-optical modulator; M, mirror; TM, translucent mirror; C, gas cell with Cs vapor; MS, magnetic shield; S, solenoid; HC, Helmholtz coils system; PBS, polarization cube; PHD1 and PHD2, balanced photodetectors. The cell C is enclosed in a thermostat (not shown in the diagram).

that confirmed that the intrinsic noise of the photodetector does not exceed shot noise.

### III. THE THEORY OF RELAXATION IN ULTRaweak FIELDS

The effects that determine the resonance width in ultraweak MFs are extremely complex; therefore, there is still no unified theory describing them under all conditions and experimental configurations, despite the enormous work done by Happer and colleagues in Refs. [27–29], by Romalis and colleagues [24,30], and subsequently systematized in Ref. [31]. Particularly poorly studied are the relaxation processes under conditions of strong modulated transverse pumping, which are becoming increasingly relevant with the development of “quiet” MEG sensors. According to Refs. [27,31] [Eqs. (2.133) and (2.134)], the longitudinal relaxation rate  $G_1 = 1/T_1$  is

$$G_1 = \frac{1}{q_N} (R_{SD} + R_{BG} + R_{OP} + R_D) + R_W, \quad (1)$$

where  $R_{SD}$  is the spin destruction rate in collisions of alkali atoms with each other,  $R_{BG}$  is the destruction rate in collisions with a buffer gas,  $R_{OP}$  is the optical pumping rate,  $R_D$  is the rate of destruction by detecting light,  $R_W$  is the rate of destruction by collisions with walls;  $q_N$  is the nuclear “slowing-down factor” equal to the ratio of the total moment of the atom to the electronic part of the moment, and dependent on the degree of polarization of the medium  $P$ : in the case of Cs,  $q_{N0} = 22$  and  $q_{N\infty} = 2I+1 = 8$  (hereinafter, index 0 corresponds to  $R_{OP} = 0$ , the index  $\infty$  corresponds to  $R_{OP} \rightarrow \infty$ );  $I$  is the atomic nuclear momentum.

Below, we will consider the resonance widths extrapolated to zero intensity of the detecting light ( $R_D \rightarrow 0$ ). The dark (i.e., extrapolated to zero pump intensity) longitudinal relaxation rate of the atomic moment is

$$R_{10} = R_{SD} + R_{BG} + R_W, \quad (2)$$

and the corresponding dark width of the MR is

$$G_{10} = \frac{1}{q_N} (R_{SD} + R_{BG}) + R_W. \quad (3)$$

According to Ref. [31] [Eq. (2.39)], in the first approximation

$$P = \frac{R_{OP}}{R_{10} + R_{OP}}. \quad (4)$$

The transverse relaxation rate  $G_2 = 1/T_2$  is

$$G_2 = G_{10} + G_{OP} + G_{SE}, \quad (5)$$

where  $G_{OP} = R_{OP}/q_N$  is the effective pump rate,  $G_{SE} = R_{SE}/q_{SE}$  is the spin-exchange broadening of the MR line,

$R_{SE}$  is the spin-exchange relaxation rate, and  $q_{SE}$  is the coefficient of suppression of spin-exchange broadening. In ultraweak fields  $q_{SE}$  tends to infinity (SERF effect), and in the strong field limit [[29], also see Ref. [31] (Eq. 2.138)] it is equal to

$$q_{SEH} = \frac{3(2I+1)^2}{2I(2I-1)} \quad (6)$$

(the index  $H$  here and below will denote the limit of a strong MF). In almost the entire range of operating temperatures and pumping intensities, the direct contribution of  $G_{10}$  to Eq. (5) can be neglected in comparison with  $G_{SE}$  and  $G_{OP}$ ; nevertheless,  $G_{10}$  plays an essential role in relaxation processes.

As the MF decreases to  $B \approx R_{SE}/\gamma$ , the SERF effect begins to manifest itself as a decrease in the MR width  $G_{SE}$  and the MR frequency  $\omega_q$ . According to Refs. [29] [Eq. (99)] and [31] [Eq. (5.5)],  $G_{SE0} = \text{Re}[\omega_{SE0}]$ ,  $\omega_{q0} = \text{Im}[\omega_{SE0}]$ , where

$$\frac{\omega_{SE0}}{R_{SE}} = M - \sqrt{-\left(\frac{\omega_L}{R_{SE}}\right)^2 - \frac{2i}{[I]} \left(\frac{\omega_L}{R_{SE}}\right) + M^2}, \quad (7)$$

$\omega_L = \gamma_B$ ,  $[I] = 2I+1$ ,  $M = ([I]^2 + 2)/(3[I])$ . Here we have rewritten this formula in a simpler form compared to Ref. [29] by normalizing frequencies to  $R_{SE}$ .

The presence of optical pumping leads to three effects: first, according to Eq. (5), it causes a linear broadening of the resonance; second, according to Eq. (3), as  $P$  increases, it causes an increase in  $G_1$  due to a decrease in  $q_N$ ; third, according to Ref. [28], at  $P \approx 1$ , it leads to light narrowing, i.e., to a decrease in the spin-exchange broadening due to the formation of a “stretched” state. In Ref. [[31], Eq. (4.9)] an approximate formula is given, obtained by expanding [31] [Eqs. (4.4)–(4.8)] into a series. It describes the light-narrowing under strong longitudinal pumping and an extremely weak radiofrequency field:

$$G_{SE} = \frac{G_{SD}}{G_{OP}} f(\omega_L, R_{SE}) G_{SE0}, \quad (8)$$

where  $f(\omega_L, \infty) = 0$ . According to Eq. (8), the spin exchange is completely suppressed under strong pumping, which is also confirmed by the numerical calculation according to Ref. [31] [Eqs. (4.4)–(4.8)].

### IV. EXPERIMENTAL INVESTIGATION OF THE RESONANCE WIDTH

We have studied the MR parameters in the range of ultraweak [ $\omega_L = (0.13 - 4.0)R_{SE}$ ] MFs at various temperatures, pump, and detection intensities. Examples of MR records at  $B = 65$  nT are shown in Figs. 2(a) and 2(b). It can be seen that in this weak field the MR cannot be

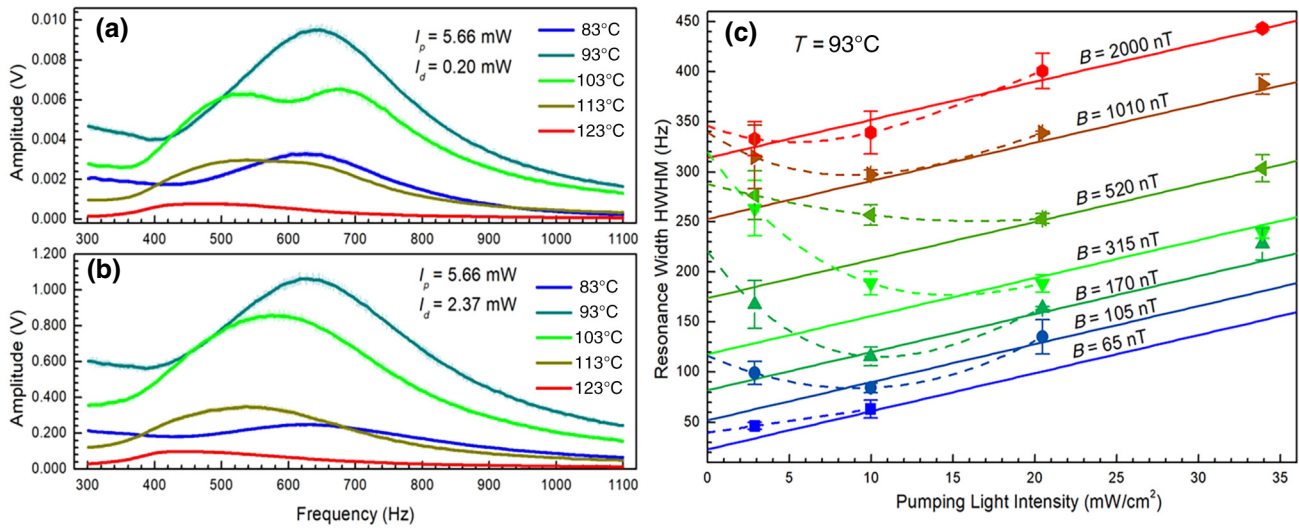


FIG. 2. (a),(b) Examples of MR recordings at  $B = 65$  nT. (c) Dependences of the MR width on the pump intensity. Each point was obtained by extrapolating the power of the detecting radiation to zero. Solid lines are the result of extrapolation of the linear part of the data sets to zero pump intensity; they are all assumed to have the same slope. Dashed lines are polynomials that approximate the nonlinear part of the data sets.

described by a Lorentzian contour for all experimental parameters; this significantly complicates the interpretation of the data and leads to an increase in errors. This is especially noticeable at low detection intensities and high temperatures, at which nonlinear absorption effects are especially pronounced [Fig. 2(a),  $T \geq 103^\circ\text{C}$ ]. As shown in Ref. [24], the reason for the distortion of the shape of resonances in the case of incomplete coincidence of the pump and interrogation zones can be atomic diffusion.

Figure 2(c) shows the experimentally measured dependences of the MR width on the pump intensity: each point is the result of extrapolation of the MR width to zero probe intensity over a series of measurements. Error values were obtained from the extrapolation dispersion.

From the data Fig. 2(c), the  $G_{\text{SE}0}$  values were obtained by approximation of the nonlinear part of the data set by polynomials of the third (where the number of experimental points allowed) or lower degree, and the  $G_{\text{SE}\infty}$  values were obtained by extrapolation of the linear part of the datasets to zero pump intensity. With linear extrapolation in accordance with Eq. (5), it was assumed that the slope of all straight lines is the same; it amounted to  $k_p = 2\pi(3.8 \pm 0.3)$  Hz  $\times$  mW $^{-1}$   $\times$  cm $^2$ . At the same time, it turns out (Fig. 6) that for all studied MF values, as well as in a wide temperature range, the  $G_{\text{SE}0}$  value (as expected) is described by Eq. (7), while the  $G_{\text{SE}\infty}$  value demonstrates an alternative unexpected dependence.

## V. EXPERIMENTAL ESTIMATION OF THE ULTIMATE SENSITIVITY

The ultimate sensitivity of the sensor can be estimated [32] based on the MR parameters based on the MR

parameters, namely the amplitude  $A$ , the width  $G = G_1 + G_2$ , and the noise spectral density  $\rho_n$ :

$$\delta B = \frac{1}{\gamma} \frac{\rho_n G}{A}. \quad (9)$$

The concept of “ultimate sensitivity” implies that only fundamental quantum noises are taken into account, that is, atomic projection noise and (for schemes with optical detection) photon shot noise [32]. The level of technical noise is considered low compared to the level of quantum noise; this condition is feasible for a wide range of MR frequencies and laser intensities. As shown in Ref. [33], the optimization of the optical detection scheme leads to an approximate equality of the spectral densities of atomic and photon noise. Hence, taking into account only the photon shot noise may lead to an overestimation of the sensitivity by no more than a factor of  $\sqrt{2}$ . The validity of this statement for various schemes of the  $M_X$  sensor was demonstrated by us in Refs. [19–21].

In practice, however, unless special precautions are taken, photon shot noise usually dominates atomic projection noise. Thus, our detection scheme is characterized by an excess of photon noise over atomic noise by about 4 times [19]. Since the noise sources are uncorrelated, the contribution of atomic noise to the spectral density of total noise is about 6%. Therefore, in what follows, by  $\rho_n$  we will mean the shot photon noise spectral density in the detection channel, which is described by the well-known expression  $\rho_n = \sqrt{2eI_{\text{ph}}\Delta f}$ ; here  $I_{\text{ph}}$  is the photocurrent,  $e$  is the charge of the electron, and  $\Delta f$  is the frequency band.

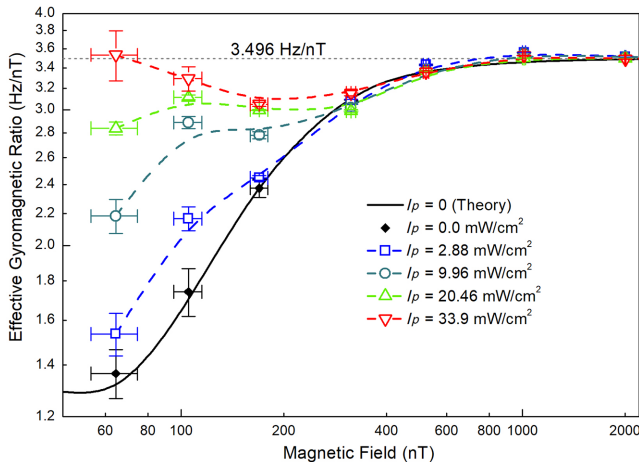


FIG. 3. Dependence of the effective gyromagnetic ratio on the MF induction for different pumping intensities: dots, experiment; solid line, calculation by Eq. (7); dashed lines are guides for the eye.

As it was shown above (Fig. 6), as the MF decreases, the resonance width decreases by an order of magnitude or more. The amplitude of the resonance in this case first slightly increases, then begins to fall. But Eq. (9) includes one more parameter—namely, the gyromagnetic ratio  $\gamma$ , which is considered a constant in strong MFs ( $\gamma = \gamma_H$ ), and which is not constant in ultraweak fields. Figure 3 shows the theoretical dependence  $\gamma(B)$  constructed from Eq. (7) and the values of  $\gamma$  measured at different pump intensities. As we can see, in the absence of pumping, the “dark” value of  $\gamma_0$  decreases with decreasing MF. The  $G_2/\gamma_0$  ratio remains approximately constant up to  $\gamma_{HB} \approx 0.3 R_{SE}$ , and only then begins to decrease. This could deprive us of any hope of improving the sensitivity, but, fortunately, the shift of the MR line by the pump light maintains the effective value of  $\gamma$  at a level close to  $\gamma_H$ .

We have studied the dependence of the ultimate sensitivity on the pump and detection intensities in a wide range of MFs and temperatures. Figure 4 shows data arrays obtained at  $B = 105$  nT. It follows from the figure that the sensitivity optimum exists for both intensities and for temperature, and with decreasing temperature, the required intensities decrease (primarily, the pump intensity). Figure 5 shows graphs of the ultimate sensitivity depending on the MF and temperature, obtained at each point by a sample from an array consisting of 16 measurements.

The graphs show a more than fourfold improvement in sensitivity in an ultraweak MF, from  $(13.2 \pm 0.2)$  fT/Hz $^{1/2}$  to  $(2.96 \pm 0.17)$  fT/Hz $^{1/2}$ . In this case, a decrease in the MF from values  $B > 1000$  nT to  $B \approx 100$  nT leads to a decrease in the required pump intensity by about a factor of 1.5 and detection intensity by a factor of 3, which should be considered an additional advantage. The signal width at the optimum point is  $(129 \pm 2)$  Hz.

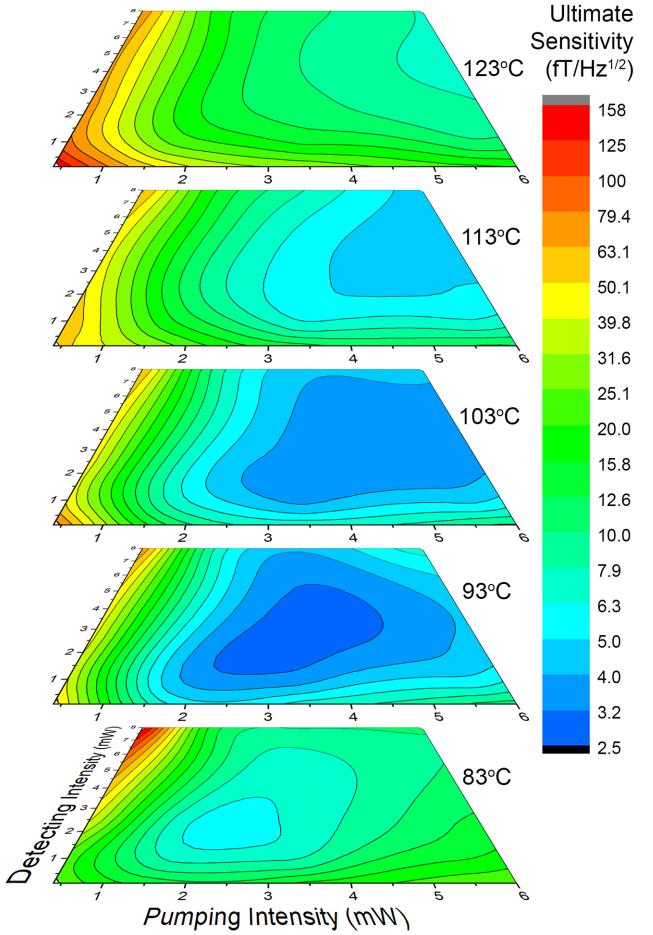


FIG. 4. Dependence of the ultimate sensitivity, estimated from the ratio of the experimentally studied resonance steepness to the calculated spectral density of shot noise, on the pump and detecting intensities and temperature.

## VI. DISCUSSION

The most unexpected result, following from the above experimental data, is that in the case of transversely modulated pumping, the spin-exchange width  $G_{SE}$  tends to a certain nonzero value  $G_{SE\infty}$  with increasing intensity. The difference between our experiment and Ref. [28] is that, instead of a weak rf field, we used modulation of the ellipticity of the pump light. This also distinguishes our experimental scheme from numerous SERF schemes (see, for example, Ref. [24]), which, like ours, use transverse pumping. Thus, the presence of  $G_{SE\infty} > 0$  is due to the modulation of the pump light, and not to its direction. The narrowing of the MR line in Cs was also studied in Ref. [34] in the scheme of an rf magnetometer with longitudinal pumping; from the data presented by the authors, it can be concluded that in their experiment the residual broadening is also not equal to zero. But since the authors do not provide data for different MF values, it is difficult to

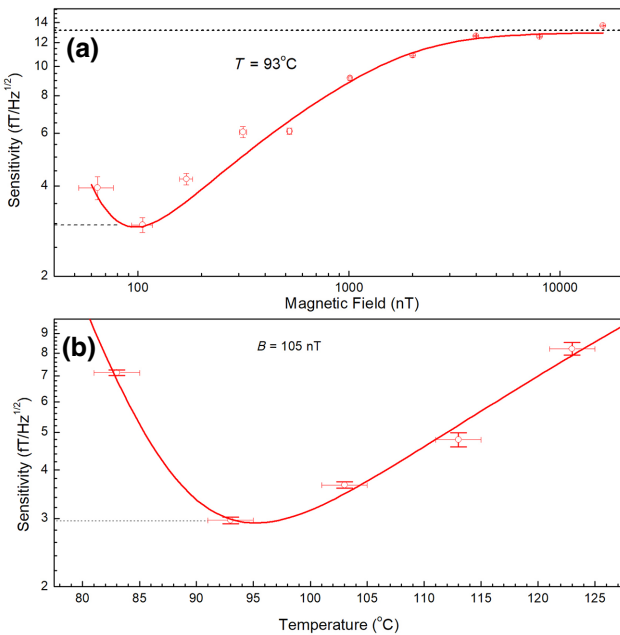


FIG. 5. Dependence of the ultimate sensitivity, estimated from the ratio of the experimentally studied resonance steepness to the calculated spectral density of shot noise (a) on the magnetic field, (b) on temperature. The dots are the experimental results, the lines are guides for the eye.

say whether this broadening is due to spin exchange or the contribution of longitudinal relaxation.

In our previous works [35] we have already noted the fact that the narrowing of the line by light in strong MF turns out to be much weaker in the Bell-Bloom scheme than in the “classical” scheme of the  $M_X$  sensor [36]. We believe that the physical nature of this limit is related to the features of the pump modulation.

The modulation of the pump ellipticity at a constant intensity should be rectangular with a constant (namely, the maximum possible) amplitude; amplitude reduction is unacceptable, because it is equivalent to mixing linear polarization with circular polarization. Therefore, the angular momentum introduced by the pump light turns out to be coaxial with the precessing atomic momentum twice per period, while in other modulation phases it makes an angle with it from  $-\pi/2$  to  $\pi/2$ . Consequently, any additional phase delay of the atomic moment will lead to the fact that part of the pump radiation will not pump, but, on the contrary, will dephase the collective moment. Under conditions close to the SERF regime, the dynamics of the system are determined by the spin-exchange rate  $R_{SE}$ : any change in external parameters (for example, the polarization of pump light) leads to the establishment of an alternative equilibrium state in the system with a characteristic time  $\Delta t = 1/R_{SE}$ , and to a phase delay  $\Delta\phi = \omega_L/R_{SE}$ . Therefore, by analogy with Eq. (4), we can introduce the

parameter of phase coherence, or phase polarization:

$$P_\phi \approx \frac{R_{SE}}{R_{SE} + \omega_L}. \quad (10)$$

Let us try to build a simple semiempirical model for the narrowing of the MR line by light. The rate of residual spin exchange  $G_{SE}$  upon narrowing of the line by light is determined by the population of the levels adjacent to the level being pumped. In the first approximation, this population is proportional to  $(1 - P)$ :

$$G_{SE} = (1 - P) G_{SE0}. \quad (11)$$

Note that, under strong pumping,  $(1 - P) = G_1/G_{OP} \approx G_{OP}/G_{SD}$ , and Eq. (11) goes over into Eq. (8) given earlier. Let us also take into account in Eq. (11) the possible dephasing of the atomic magnetic moment by pump modulation. The MR broadening  $G_M$  introduced by the modulation should be zero in the absence of pumping, and constant with strong pumping. Therefore, we can assume that  $G_M$  is proportional to  $P$ . As follows from Fig. 6(a), the value of  $G_M$  in weak fields increases in proportion to the modulation frequency and saturates at the level  $G_{SEH} = R_{SEH}/q_{SEH}$  at  $\omega_L \approx R_{SEH}$ . Therefore, we can also assume that  $G_M \sim (1 - P_\phi)$ :

$$G_{SE} = (1 - P') G_{SE0} + P (1 - P_\phi)^m G_{SE0}. \quad (12)$$

Empirical parameters  $n$  and  $m$  are introduced here in order to more adequately describe a multilevel system, for which the polarization coefficients are determined differently than for a two-level one. The result of the approximation of the experimental data by Eqs. (7) and (12) at  $n = 1.95$ ,  $m = 1.1$  is shown in Fig. 6. It should be noted that the data obtained in an MF with an induction of more than 2000 nT reveal other effects, in particular, an increase in the coefficient  $k_p$ . These effects are outside the scope of this paper and will not be discussed here.

An example of the dependence of the total resonance width  $G_2$  and individual contributions to the width on the pumping rate calculated in our model is shown in Fig. 7; in addition, Fig. 7 shows the dependence of the total width  $G_{WH}$ , calculated by the formulas Eqs. (4.4)–(4.8) from Ref. [31]. It follows from Eqs. (7) and (12) that under transverse modulated pumping, the spin-exchange broadening in weak fields can be reduced by a maximum of a factor of 3 by pumping light. On the other hand, according to Ref. [31], the total resonance width (which includes broadening by pumping light  $G_{OP}$ ), in Cs can be reduced by the longitudinal pump light by a factor of 8. But as one can see, it decreases by no more than a factor of 2 in the Bell-Bloom configuration.

As we suggested above, the residual broadening by modulation can be due to two factors: (1) the width of

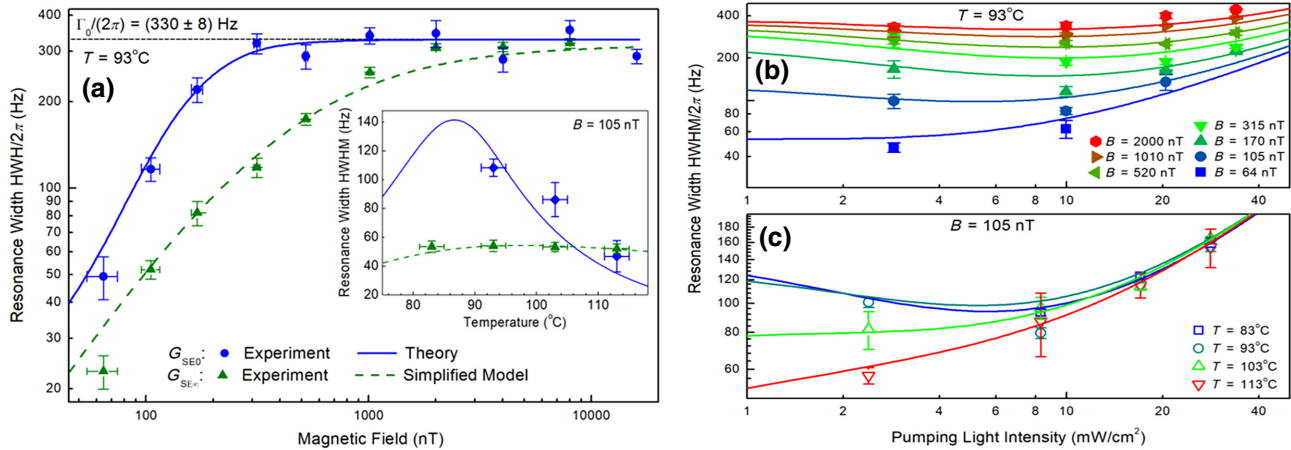


FIG. 6. (a) Dependence of the dark ( $G_{SE0}$ ) and maximally light-reduced ( $G_{SE\infty}$ ) spin-exchange relaxation rates as functions of the MF; points, experiment; lines, calculation by Eqs. (7) and (12). The inset shows the same values depending on the temperature. (b) Dependences of the magnetic resonance width on the pump intensity at  $T = 93$  °C for several values of the MF induction; solid lines, calculation by Eq. (12). (c) The same values at  $B = 105$  nT for several temperatures.

the distribution of the phase of the modulation itself (from  $-\pi/2$  to  $+\pi/2$ ) with respect to the phase of the fundamental harmonic of the modulation, and (2) the phase delay of the atomic moment with respect to the fundamental harmonic of the modulation. Note that the most obvious assumption that the side spectral components of the modulated radiation are the broadening factor does not work, since these components lie far beyond the width of the MR line. In order to find out which of the two factors is decisive, we carried out an additional experiment, replacing the modulation of the pump ellipticity by the modulation of

its intensity. In this case, pumping was carried out once per period of the Larmor frequency by a pulse with constant circular polarization and variable duration (from 10 to 50%). The resonance width was measured as a function of the pulse duration at a constant average pump intensity. At  $B = 105$  nT, the maximum broadening by a long pulse was  $(13.0 \pm 7.5)$  Hz, which is an insignificant part of the residual broadening  $G_{SE\infty} = (52 \pm 4)$  Hz.

At  $B = 2000$  nT, the maximum broadening by a long pulse turned out to be indistinguishable within the error. Thus, we have shown that factor (1) is not decisive, and the residual broadening is caused by the phase shift of the momentum precession with respect to the pump.

Even taking into account the incomplete light narrowing of the MR line, the results presented above demonstrate a significant advantage of ultraweak MFs for the operation of an  $M_X$  sensor built according to the Bell-Bloom scheme. However, there are two negative factors that should be taken into account: firstly, a decrease in line width means a decrease in instrument performance; secondly, lowering the MR frequency to hundreds of hertz makes the sensor potentially more sensitive to low-frequency technical noises of the laser, and, accordingly, requires special measures to suppress these noises (signal frequency transfer by modulation of the detecting light can be used as one such measure) [37–39].

In other words, decreasing the MF value and the accompanying decrease in MR linewidth causes the same problems in  $M_X$  sensors that SERF sensors face. The balanced recording scheme used in our experiment is capable of suppressing the laser intensity noise by 1 to 2 orders of magnitude compared to simple recording of the transmitted light intensity used in SERF compact sensors, but this is achieved at the expense of the scheme complexity.

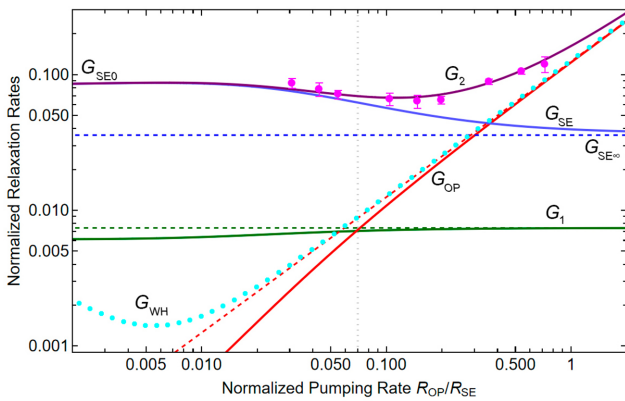


FIG. 7. An example of the dependence of the calculated [by Eqs. (7)–(12)] MR width on the effective pumping rate (black line) and its comparison with experiment (magenta dots).  $R_{WH}$ —calculation by Eqs. (4.4)–(4.8) from Ref. [31]; other designations are given in the text. All quantities are normalized to the spin-exchange rate  $R_{SE}$ . Calculation parameters:  $T = 93$  °C,  $B = 105$  nT,  $\omega_L = (2\pi)367$  Hz. Calculated relaxation rates:  $R_{SE} = (2\pi)1438$  Hz,  $G_{SE0} = (2\pi)119$  Hz,  $G_{SE\infty} = (2\pi)52$  Hz,  $G_W = (2\pi)7.7$  Hz,  $R_{SD} = (2\pi)10.3$  Hz,  $R_{BG} = (2\pi)13.3$  Hz.

In addition, when discussing the practical applicability of the proposed scheme, one should take into account the problems, which are common to nonzero field optical sensors. Firstly, the sensitivity axis of such a sensor is determined by the MF direction. On the one hand, this complicates the use of such sensors in wearable MEG systems, on the other hand, it makes it possible to change the sensitivity axis during the procedure simply by changing this direction. The Bell-Bloom scheme with co-directed beams perpendicular to the MF vector has an advantage over schemes with longitudinal pumping, since it remains operational when the sensor is rotated through an angle from 0 to  $360^\circ$  around the  $x$  axis specified by the direction of the beams (see Fig. 1). The dependence of the sensitivity on this angle is determined by the degree of absorption of the linearly polarized probe beam. In a two-beam scheme, this dependence can be made arbitrarily weak (while keeping other parameters constant) by simultaneously increasing detuning and intensity of the detecting beam. As for the rotation around the  $y$  axis, the sensitivity turns out to be proportional to the square of the sine of this angle between the direction of the beams and the MF vector. This is explained by the fact that both the pumping and the detection efficiencies are proportional to the sine of this angle. In practice, this means that deviations of  $\pm 15^\circ$  will lead to a decrease in sensitivity by 10%.

Further, it should be taken into account that in order to achieve the ultimate sensitivity, it is essential to maintain the MR amplitude at a certain level. The strongest dependence of the MR amplitude on the MF is observed in weak MFs. At the parameters corresponding to the best sensitivity in our experimental configuration (see Fig. 5), the variations leading to a change in the signal amplitude by 10% are  $\Delta T = 2.9^\circ\text{C}$  (which is easily fulfilled in a controllable thermostat), and  $\Delta B = 8.5 \text{ nT}$ . It follows from this that certain measures must be taken in order to limit the variations in the MF at the location of each sensor to the desired level.

## VII. CONCLUSIONS

We have demonstrated the fundamental performance of the Bell-Bloom  $M_X$  sensor in ultraweak magnetic fields and showed that its sensitivity can be improved to reach that of a SERF sensor, while retaining most of the advantages and disadvantages of the  $M_X$  scheme. Among these advantages is the absence of radiofrequency interference, among the disadvantages is the inability to simultaneously measure more than one component of the MEG signal. In addition, in ultraweak fields, the speed of the sensor decreases and the level of technical noise increases, which requires special precautions. On the other hand, in ultraweak field, the  $M_X$  sensor requires substantially lower intensities for pumping and detection. We also showed that spin-exchange relaxation under conditions of transversely

modulated pumping has its own peculiarities and gave an empirical description of them.

The authors declare that they have no conflict of interest.

- 
- [1] D. Cohen, Magnetoencephalography: Detection of the brain's electrical activity with a superconducting magnetometer, *Science* **175**, 664 (1972).
  - [2] M. J. Brookes, J. Leggett, M. Rea, R. M. Hill, N. Holmes, E. Boto, and R. Bowtell, Magnetoencephalography with optically pumped magnetometers (OPM-MEG): The next generation of functional neuroimaging, *Trends Neurosci.* **45**, 621 (2022).
  - [3] J. Iivanainen, M. Stenroos, and L. Parkkonen, Measuring MEG closer to the brain: Performance of on-scalp sensor arrays, *NeuroImage* **147**, 542 (2017).
  - [4] J. Iivanainen, R. Zetter, and L. Parkkonen, Potential of on-scalp MEG: Robust detection of human visual gamma-band responses, *Hum. Brain Mapp.* **41**, 150 (2020).
  - [5] I. K. Kominis, T. W. Kornack, J. C. Allred, and M. V. Romalis, A subfemtotesla multichannel atomic magnetometer, *Nature* **422**, 596 (2003).
  - [6] M. Rea, E. Boto, N. Holmes, R. Hill, J. Osborne, N. Rhodes, J. Leggett, L. Rier, R. Bowtell, and V. Shah, *et al.*, A 90-channel triaxial magnetoencephalography system using optically pumped magnetometers, *Annals of the New York Academy of Sciences* (2022).
  - [7] E. Boto, S. S. Meyer, V. Shah, O. Alem, S. Knappe, P. Kruger, T. M. Fromhold, M. Lim, P. M. Glover, P. G. Morris, R. Bowtell, G. R. Barnes, and M. J. Brookes, A new generation of magnetoencephalography: Room temperature measurements using optically-pumped magnetometers, *NeuroImage* **149**, 404 (2017).
  - [8] K.-M. C. Fu, G. Z. Iwata, A. Wickenbrock, and D. Budker, Sensitive magnetometry in challenging environments, *AVS Quantum Sci.* **2**, 044702 (2020).
  - [9] N. V. Nardelli, A. R. Perry, S. P. Krzyzewski, and S. A. KnappeSEP, A conformal array of microfabricated optically-pumped first-order gradiometers for magnetoencephalography, *EPJ Quantum Technol.* **7**, 11 (2020).
  - [10] M. Limes, E. Foley, T. Kornack, S. Caliga, S. McBride, A. Braun, W. Lee, V. Lucivero, and M. Romalis, Portable magnetometry for detection of biomagnetism in ambient environments, *Phys. Rev. Appl.* **14**, 011002(R) (2020).
  - [11] E. Boto, V. Shah, R. M. Hill, N. Rhodes, J. Osborne, C. Doyle, N. Holmes, M. Rea, J. Leggett, and R. Bowtell, *et al.*, Triaxial detection of the neuromagnetic field using optically-pumped magnetometry: Feasibility and application in children, *NeuroImage* **252**, 119027 (2022).
  - [12] A. L. Bloom, Principles of operation of the rubidium vapor magnetometer, *Appl. Opt.* **1**, 61 (1962).
  - [13] V. Schultze, B. Schillig, R. IJsselsteijn, T. Scholtes, S. Woetzel, and R. Stolz, An optically pumped magnetometer working in the light-shift dispersed Mz mode, *Sensors* **17**, 561 (2017).
  - [14] Y. Guo, S. Wan, X. Sun, and J. Qin, Compact, high-sensitivity atomic magnetometer utilizing the light-narrowing effect and in-phase excitation, *Appl. Opt.* **58**, 734 (2019).

- [15] R. Zhang, W. Xiao, Y. Ding, Y. Feng, X. Peng, L. Shen, C. Sun, T. Wu, Y. Wu, Y. Yang, Z. Zheng, X. Zhang, J. Chen, and H. Guo, Recording brain activities in unshielded earth's field with optically pumped atomic magnetometers, *Sci. Adv.* **6**, eaba8792 (2020).
- [16] O. Alem, K. J. Hughes, I. Buard, T. P. Cheung, T. Maydew, A. Griesshammer, K. Holloway, A. Park, V. Lechuga, and C. Coolidge, *et al.*, An integrated full-head OPM-MEG system based on 128 zero-field sensors, *Front. Neurosci.* **17**, 1014 (2023).
- [17] I. Fescenko, P. Knowles, A. Weis, and E. Breschi, A Bell-Bloom experiment with polarization-modulated light of arbitrary duty cycle, *Opt. Express* **21**, 15121 (2013).
- [18] Z. D. Grujic and A. Weis, Atomic magnetic resonance induced by amplitude-, frequency-, or polarization-modulated light, *Phys. Rev. A* **88**, 012508 (2013).
- [19] M. V. Petrenko, A. S. Pazgalev, and A. K. Vershovskii, Single-beam all-optical non-zero field magnetometric sensor for magnetoencephalography applications, *Phys. Rev. Appl.* **15**, 064072 (2021).
- [20] M. V. Petrenko, S. P. Dmitriev, A. S. Pazgalev, A. E. Ossadtchi, and A. K. Vershovskii, Towards the non-zero field cesium magnetic sensor array for magnetoencephalography, *IEEE Sensors Journal* (2021).
- [21] M. V. Petrenko, A. S. Pazgalev, and A. K. Vershovskii, All-optical nonzero-field vector magnetic sensor for magnetoencephalography, *Phys. Rev. Appl.* **20**, 024001 (2023).
- [22] E. N. Popov, V. A. Bobrikova, S. P. Voskoboinikov, K. A. Barantsev, S. M. Ustinov, A. N. Litvinov, A. K. Vershovskii, S. P. Dmitriev, V. A. Kartoshkin, A. S. Pazgalev, and M. V. Petrenko, Features of the formation of the spin polarization of an alkali metal at the resolution of hyperfine sublevels in the  $^2S_{1/2}$  state, *JETP Lett.* **108**, 513 (2018).
- [23] T. Scholtes, V. Schultze, R. IJsselsteijn, S. Woetzel, and H.-G. Meyer, Light-narrowed optically pumped  $m_x$  magnetometer with a miniaturized Cs cell, *Phys. Rev. A* **84**, 043416 (2011).
- [24] M. P. Ledbetter, I. M. Savukov, V. M. Acosta, D. Budker, and M. V. Romalis, Spin-exchange-relaxation-free magnetometry with Cs vapor, *Phys. Rev. A* **77**, 033408 (2008).
- [25] A. Fairweather and M. Usher, A vector rubidium magnetometer, *J. Phys. E: Sci. Instrum.* **5**, 986 (1972).
- [26] A. K. Vershovskii, Project of laser-pumped quantum  $M_X$  magnetometer, *Tech. Phys. Lett.* **37**, 140 (2011).
- [27] S. Appelt, A. B.-A. Baranga, C. J. Erickson, M. V. Romalis, A. R. Young, and W. Happer, Theory of spin-exchange optical pumping of  $^3\text{He}$  and  $^{129}\text{Xe}$ , *Phys. Rev. A* **58**, 1412 (1998).
- [28] S. Appelt, A. B. A. Baranga, A. R. Young, and W. Happer, Light narrowing of rubidium magnetic-resonance lines in high-pressure optical-pumping cells, *Phys. Rev. A* **59**, 2078 (1999).
- [29] W. Happer and A. C. Tam, Effect of rapid spin exchange on the magnetic-resonance spectrum of alkali vapors, *Phys. Rev. A* **16**, 1877 (1977).
- [30] I. M. Savukov and M. V. Romalis, Effects of spin-exchange collisions in a high-density alkali-metal vapor in low magnetic fields, *Phys. Rev. A* **71**, 023405 (2005).
- [31] S. J. Seltzer, *Developments in alkali-metal atomic magnetometry*, Ph.D., Princeton University (2008).
- [32] D. Budker and M. Romalis, Optical magnetometry, *Nat. Phys.* **3**, 227 (2007).
- [33] A. K. Vershovskii, S. P. Dmitriev, G. G. Kozlov, A. S. Pazgalev, and M. V. Petrenko, Projection spin noise in optical quantum sensors based on thermal atoms, *Tech. Phys.* **65**, 1193 (2020).
- [34] Y. Fu, X. Liu, and J. Yuan, Light narrowing of cesium magnetic-resonance lines in a radio-frequency atomic magnetometer, *AIP Adv.* **9**, 015304 (2019).
- [35] A. K. Vershovskii and M. V. Petrenko, Three-level approximation upon calculating the parameters of optically detected magnetic resonance under the conditions of intense laser pumping, *Opt. Spectrosc.* **129**, 501 (2021).
- [36] D. Budker and D. F. J. Kimball, *Optical Magnetometry* (Cambridge University Press, Cambridge, 2013).
- [37] D. Budker, D. F. Kimball, V. V. Yashchuk, and M. Zolotorev, Nonlinear magneto-optical rotation with frequency-modulated light, *Phys. Rev. A* **65**, 055403 (2002).
- [38] S. Pustelny, W. Gawlik, S. Rochester, D. J. Kimball, V. Yashchuk, and D. Budker, Nonlinear magneto-optical rotation with modulated light in tilted magnetic fields, *Phys. Rev. A* **74**, 063420 (2006).
- [39] A. K. Vershovskii and M. V. Petrenko, Frequency transfer of an optically detected magnetic resonance and observation of the Hanle effect in a nonzero magnetic field, *Opt. Spectrosc.* **131**, 3 (2023).